Numerical Analysis of the Rectangular Dielectric Waveguide and Its Modifications

KAZUHIKO OGUSU, MEMBER, IEEE

Abstract—**Dielectric waveguides suitable for millimeter and submillimeter wave integrated circuits are analyzed by applying the generalized telegraphist's equations. The dielectric waveguides treated in this paper are the rectangular dielectric image line, the cladded rectangular dielectric image line, the insulated image guide, and the strip dielectric guide. Numerical results of the propagation constant, the power distribution, and the field configuration in these dielectric waveguides are presented. Values for the propagation constants obtained by our method are compared with other theoretical results. Although this work is based on a closed waveguide model, it may be applicable to wide classes of dielectric waveguides with arbitrary dielectric profiles and cross sections.**

I. Introduction

IN RECENT YEARS dielectric waveguides have been used as transmission media at millimeter and submillimeter wave frequencies. The rectangular dielectric waveguide and its modifications have been extensively studied because of their compatibility with integrated circuits.

Fig. 1 shows the cross sections of several dielectric waveguides with a conducting ground plane; these are interesting for physical and theoretical reasons. If we consider the image of the field reflected by the conducting ground plane, the dielectric waveguides shown in Fig. 1(a), (b), and (d) become the rectangular dielectric waveguide [1]–[6], the cladded rectangular dielectric waveguide, and the single material fiber [13], respectively. The cladded rectangular dielectric waveguide has the advantage that the power carried by the guide is protected from the influence of the environment. The insulated image guide ($\varepsilon_r > \varepsilon_t$) shown in Fig. 1(c) has been proposed to reduce conductor losses of the rectangular dielectric image line. By contraries, the dielectric waveguide with $\varepsilon_t > \varepsilon_r$ in Fig. 1(c) is called the strip dielectric guide [14]. On the other hand, dielectric waveguides for optical integrated circuits, which have a dielectric substrate instead of a conducting ground plane, have been investigated by a number of authors [9]–[14].

Although the dispersion characteristics of these dielectric waveguides may be determined relatively easily, detailed information about the field distributions, especially within the dielectric waveguides, is rarely reported. But, an experimental technique, which is applicable to detect the field distributions within wide classes of dielectric waveguides, has recently been proposed by Itoh [15]. The author has theoretically studied the transmission characteristics of the rectangular dielectric waveguide by applying the generalized telegraphist's equations [7] and has experimentally shown that this analysis yields good results for open dielectric waveguides even though it has been based on a closed waveguide model [8]. The method has the advantage that it may be applicable to wide classes of dielectric waveguides with arbitrary dielectric profiles and cross sections.

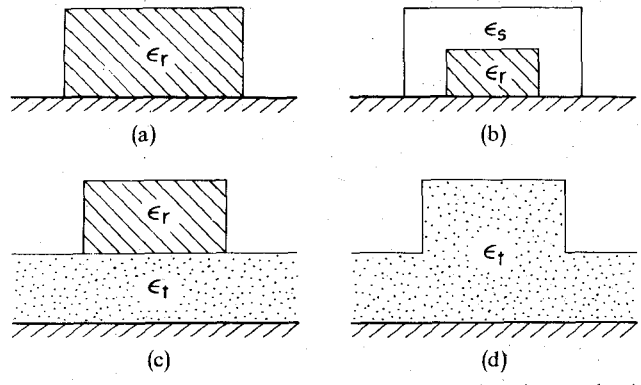

Fig. 1. Cross sections of dielectric waveguides with the conducting ground plane. (a) Rectangular dielectric image line. (b) Cladded rectangular dielectric image line. (c) Insulated image guide ($\varepsilon_r > \varepsilon_t$). Strip dielectric guide ($\varepsilon_r < \varepsilon_t$). (d) Dielectric image line corresponding to the single material fiber.

The purpose of this paper is to determine the field distribution for various kinds of dielectric waveguides to provide the basic knowledge of their physical properties using the generalized telegraphist's equations. Numerical results presented in this paper include dispersion characteristics, lines of force, and equicontours of the electromagnetic power density. These data will be useful in developing new waveguide systems and in checking new analytical techniques for solving similar problems. For the justification of the present analysis, the author is going to report more detailed experimental results including the field distributions within these dielectric waveguides.

II. Method of Analysis

Since the details of the method of analysis based on the generalized telegraphist's equations may be found in [7] and [16], we shall here describe the method only briefly. For the sake of analysis, we enclose the open dielectric waveguide with a metallic wall as shown in Fig. 2. The dielectric waveguides shown in Fig. 1 are obtained from the somewhat generalized waveguide structure in Fig. 2, when the wall is removed. This treatment is valid for surface waves, of which most of the power carried is concentrated in the dielectric

Manuscript received February 9, 1977; revised May 20, 1977.

The author is with the Faculty of Engineering, Shizuoka University, Johoku 3-5-1, Hamamatsu, 432 Japan.

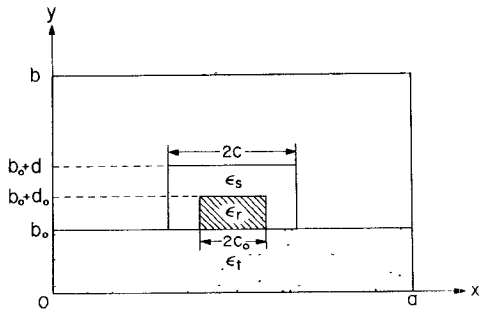

Fig. 2. Cross section of the generalized dielectric waveguide for the analysis.

medium. This shielded dielectric waveguide may also be regarded as the metallic waveguide containing an inhomogeneous dielectric medium. We assume that the permittivity ε of the medium is a function of the transverse coordinates x and y, and that the permeability μ is that of the free space.

First, in order to apply the generalized telegraphist's equations to this problem, we eliminate the longitudinal field component from Maxwell's equations and obtain

$$\frac{\partial \boldsymbol{E}_t}{\partial z} = \frac{1}{j\omega} \nabla_t \left(\frac{1}{\varepsilon} \nabla_t \cdot (\boldsymbol{H}_t \times \boldsymbol{a}_z) \right) - j\omega\mu (\boldsymbol{H}_t \times \boldsymbol{a}_z) \tag{1}$$

$$\frac{\partial \boldsymbol{H}_t}{\partial z} = \frac{1}{j\omega\mu} \nabla_t \nabla_t \cdot (\boldsymbol{a}_z \times \boldsymbol{E}_t) - j\omega\varepsilon (\boldsymbol{a}_z \times \boldsymbol{E}_t) \tag{2}$$

where ω is the angular frequency, $\boldsymbol{a}_z$ is the unit vector in the z direction, $\nabla_t = \nabla - \boldsymbol{a}_z(\partial/\partial z)$ is the two-dimensional del operator, and the subscript t denotes the transverse components.

In general, unknown transverse electromagnetic fields $\boldsymbol{E}_t$ and $\boldsymbol{H}_t$ may be expanded in terms of orthogonal mode functions $\boldsymbol{e}(x,y)$ and $\boldsymbol{h}(x,y)$ of the empty metallic waveguide as

$$\boldsymbol{E}_t = \sum_i^\infty V_{(i)}(z)\boldsymbol{e}_{(i)}(x,y) + \sum_j^\infty V_{[j]}(z)\boldsymbol{e}_{[j]}(x,y) \tag{3}$$

$$\boldsymbol{H}_t = \sum_i^\infty I_{(i)}(z)\boldsymbol{h}_{(i)}(x,y) + \sum_j^\infty I_{[j]}(z)\boldsymbol{h}_{[j]}(x,y) \tag{4}$$

where $V(z)$ and $I(z)$ are mode voltages and mode currents to be determined, respectively, the subscript in parentheses denotes the TM mode, the subscript in brackets denotes the TE mode, and i and j denote double index such as mn. The mode functions are defined by the following scalar functions $\phi_{(i)}(x,y)$ and $\psi_{[j]}(x,y)$:

$$\left.\begin{aligned} \boldsymbol{e}_{(i)}(x,y) &= -\nabla_t \phi_{(i)}(x,y) \\ \boldsymbol{h}_{(i)}(x,y) &= -\boldsymbol{a}_z \times \nabla_t \phi_{(i)}(x,y) \end{aligned}\right\} \quad \text{for TM modes} \tag{5}$$

$$\left.\begin{aligned} \boldsymbol{e}_{[j]}(x,y) &= \boldsymbol{a}_z \times \nabla_t \psi_{[j]}(x,y) \\ \boldsymbol{h}_{[j]}(x,y) &= -\nabla_t \psi_{[j]}(x,y) \end{aligned}\right\} \quad \text{for TE modes} \tag{6}$$

where $\phi_{(i)}(x,y)$ and $\psi_{[j]}(x,y)$ are solutions of the following two-dimensional Helmholtz equation

$$(\nabla_t^2 + k_c^2) \begin{Bmatrix} \phi(x,y) \\ \psi(x,y) \end{Bmatrix} = 0 \tag{7}$$

and individually satisfy the boundary conditions on the waveguide wall, and where k_c is the cutoff wavenumber of the mn mode and is given by

$$k_c = \sqrt{\left(\frac{m\pi}{a}\right)^2 + \left(\frac{n\pi}{b}\right)^2}. \tag{8}$$

These scalar functions may be founded in [17].

Next, we will derive the generalized telegraphist's equations for the mode voltages and mode currents. After substituting (3) and (4) into (1) and (2), we take the inner products with the known mode functions $\boldsymbol{e}_{(i)}(x,y)$, $\boldsymbol{h}_{(i)}(x,y)$, $\boldsymbol{e}_{[j]}(x,y)$, and $\boldsymbol{h}_{[j]}(x,y)$ for different values of i and j. Using the orthogonality property of the mode functions and the two-dimensional Green's theorem, we obtain the following generalized telegraphist's equations

$$\frac{dV_{(n)}(z)}{dz} = -\frac{1}{j\omega\varepsilon_0} \sum_i^\infty Z_1(n,i) I_{(i)}(z) - j\omega\mu I_{(n)}(z) \tag{9}$$

$$\frac{dV_{[m]}(z)}{dz} = -j\omega\mu I_{[m]}(z) \tag{10}$$

$$\frac{dI_{(n)}(z)}{dz} = -j\omega\varepsilon_0 \left(\sum_i^\infty Y_1(n,i) V_{(i)}(z) + \sum_j^\infty Y_2(n,j) V_{[j]}(z) \right) \tag{11}$$

$$\frac{dI_{[m]}(z)}{dz} = -j\omega\varepsilon_0 \left(\sum_i^\infty Y_3(m,i) V_{(i)}(z) + \sum_j^\infty Y_4(m,j) V_{[j]}(z) \right) - \frac{k_{c[m]}^2}{j\omega\mu} V_{[m]}(z) \tag{12}$$

where the coefficients are given as

$$\begin{aligned} Z_1(n,i) &= k_{c(i)}^2 k_{c(n)}^2 \iint \frac{1}{\varepsilon_r(x,y)} \phi_{(i)}(x,y)\phi_{(n)}(x,y)\, dS \\ Y_1(n,i) &= \iint \varepsilon_r(x,y) \boldsymbol{h}_{(i)}(x,y) \cdot \boldsymbol{h}_{(n)}(x,y)\, dS \\ Y_2(n,j) &= \iint \varepsilon_r(x,y) \boldsymbol{h}_{[j]}(x,y) \cdot \boldsymbol{h}_{(n)}(x,y)\, dS \\ Y_3(m,i) &= \iint \varepsilon_r(x,y) \boldsymbol{h}_{(i)}(x,y) \cdot \boldsymbol{h}_{[m]}(x,y)\, dS \\ Y_4(m,j) &= \iint \varepsilon_r(x,y) \boldsymbol{h}_{[j]}(x,y) \cdot \boldsymbol{h}_{[m]}(x,y)\, dS \end{aligned} \tag{13}$$

and where $\varepsilon_r(x,y) = \varepsilon(x,y)/\varepsilon_0$ is the relative permittivity, and the integration is over the metallic waveguide cross section. The above derivation process is generally known as Galerkin's procedure.

Now we consider the sinusoidal propagation expressed as $V_{(i)}(z) = V_{(i)} e^{-jk_z z}$, $V_{[j]}(z) = V_{[j]} e^{-jk_z z}$, where k_z is the unknown propagation constant. Approximating (3) and (4) by N terms for the TM mode and M terms for the TE mode, and eliminating the mode currents from the generalized telegraphist's equations, we have the following characteristic eigenvalue equation:

$$\begin{bmatrix} a_{11} & a_{12} & \cdots & a_{1N+M} \\ a_{21} & a_{22} & & \\ \vdots & & & \vdots \\ a_{N+M1} & \cdots & & a_{N+MN+M} \end{bmatrix} \begin{bmatrix} V_{(1)} \\ \vdots \\ V_{(N)} \\ V_{[1]} \\ \vdots \\ V_{[M]} \end{bmatrix} = k_z^2 \begin{bmatrix} V_{(1)} \\ \vdots \\ V_{(N)} \\ V_{[1]} \\ \vdots \\ V_{[M]} \end{bmatrix} \tag{14}$$

where the elements a_{ij} $(i,j = 1, 2, \cdots, N + M)$ of the matrix are functions of the dielectric profile and the cross section of the dielectric waveguide. Once a_{ij}'s are obtained, we can solve (14) for the eigenvalue k_z^2 and eigenvectors $V_{(1)}, \cdots, V_{(N)}, V_{[1]}, \cdots, V_{[M]}$. If the metallic wall is large enough, the range of the normalized propagation constant k_z/k_0 for the surface waves is between 1 and $\sqrt{\varepsilon_r \max}$, where $\varepsilon_r \max$ is the maximum relative permittivity of the dielectric medium. On the other hand, mode voltage and mode current are related as

$$V_{(i)} = z_{(i)} I_{(i)} \qquad z_{(i)} = \frac{\sqrt{k_0^2 - k_{c(i)}^2}}{\omega \varepsilon_0} \tag{15}$$

$$V_{[j]} = z_{[j]} I_{[j]} \qquad z_{[j]} = \frac{\omega \mu}{\sqrt{k_0^2 - k_{c[j]}^2}} \tag{16}$$

where $k_0 = \omega\sqrt{\varepsilon_0 \mu}$ is the free-space wavenumber. Once the eigenvalues and their eigenvectors are obtained, we can calculate the field components $\boldsymbol{E}_t$, E_z, $\boldsymbol{H}_t$, and H_z of the corresponding normal modes of the shielded dielectric waveguide and obtain the power flow from

$$P = \tfrac{1}{2} \operatorname{Re} (\boldsymbol{E}_t \times \boldsymbol{H}_t^*). \tag{17}$$

Finally, since the generalized telegraphist's equations are derived through Galerkin's procedure, the resulting expression for the propagation constant becomes stationary. This is one of the advantages of the present method. Another advantage of the method is that it is applicable to dielectric waveguides with arbitrary cross sections and profiles.

III. Numerical Results and Discussion

The normal modes of the dielectric waveguides shown in Fig. 1 are grouped in two families, E_{pq}^y and E_{pq}^x [2]. The main field components of the first family are E_y and H_x, while those of the second family are E_x and H_y. The subscripts p and q denote the number of extrema of the electric or magnetic field in the x and y directions, respectively. The lowest order E^y mode of the dielectric waveguides is the E_{11}^y mode in which E_y is symmetric about $x = a/2$. We must expand (3) and (4) by taking into account such symmetry of the field.

In this section we present numerical results for the dielectric waveguides shown in Fig. 1. For all results of the power distribution, the power is normalized so that the total transmission power is unity when the half width c of the dielectric strip is chosen the unit length. These results are valid for the rectangular dielectric waveguide, the cladded rectangular dielectric waveguide, and the single material fiber, which are electrically equivalent to those shown in Fig. 1.

Rectangular Dielectric Image Line

The rectangular dielectric image line shown in Fig. 1(a) is a special case with $b_0 = 0$, $c_0 = c$, and $d_0 = d$ in Fig. 2. If we take into account the image of the field reflected by the conducting ground plane, it becomes the rectangular dielectric waveguide. But, the E_{pq}^y (where q is an even number) modes of the rectangular dielectric waveguide can not be obtained. If necessary, they can be obtained by setting the dielectric core at the center of the metallic waveguide. The dispersion characteristics of this dielectric waveguide have previously been evaluated by many authors [1]–[7]. The propagation constants obtained by our method are stationary. Table I shows the comparison of the propagation constant computed with different matrix sizes to estimate the accuracy of our method for computing the propagation constants. In this approximation, (3) and (4) are truncated with N_0 terms in the x and y directions for both the TE and TM modes, and the resulting matrix size of (14) is $2N_0^2 \times 2N_0^2$. Even $N_0 = 5$ is sufficient to give good results. On the other hand, it is difficult to estimate the influence of the metallic wall on the propagation constant. But, since normal modes are surface waves, only a small amount of the total power flows outside the dielectric waveguide. By increasing the distance between the interface of the dielectric waveguide and the metallic wall, and correspondingly increasing the matrix size, good results can be obtained.

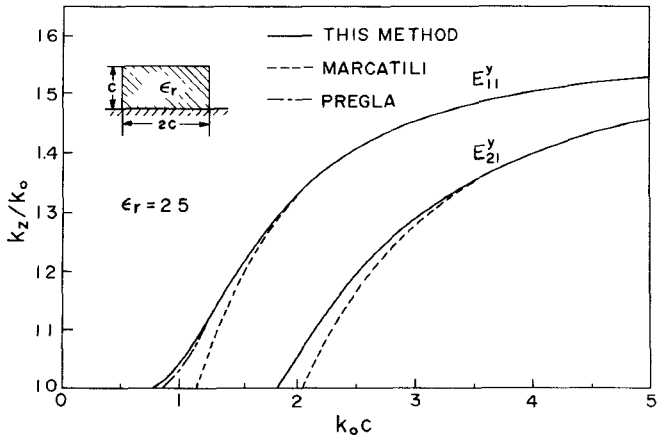

Fig. 3. Dispersion characteristics for the E_{11}^y and E_{21}^y modes in the rectangular dielectric image line with $d/c = 1.0$ and $\varepsilon_r = 2.5$ $(N_0 = 5)$.

TABLE I
Comparison of the Propagation Constant in the Rectangular Dielectric Image Line with Different Matrix Sizes: $\varepsilon_r = 2.5$, $k_0 c = 5.0$, $a/c = 5.0$, $d/c = 1.0$, $b/d = 2.5$

Matrix Size	Propagation Constant K_Z/K_0	
	$E^Y{}_{11}$ mode	$E^Y{}_{21}$ mode
2×4^2	1.527	1.452
2×5^2	1.529	1.456
2×6^2	1.529	1.458
2×7^2	1.529	1.459

Fig. 3 shows the dispersion characteristics for the E_{11}^y and E_{21}^y modes in the rectangular dielectric image line with the aspect ratio $d/c = 1.0$ and the relative permittivity $\varepsilon_r = 2.5$. In this calculation $N_0 = 5$ was used. For the waveguide with parameters close to the transition region, that is near

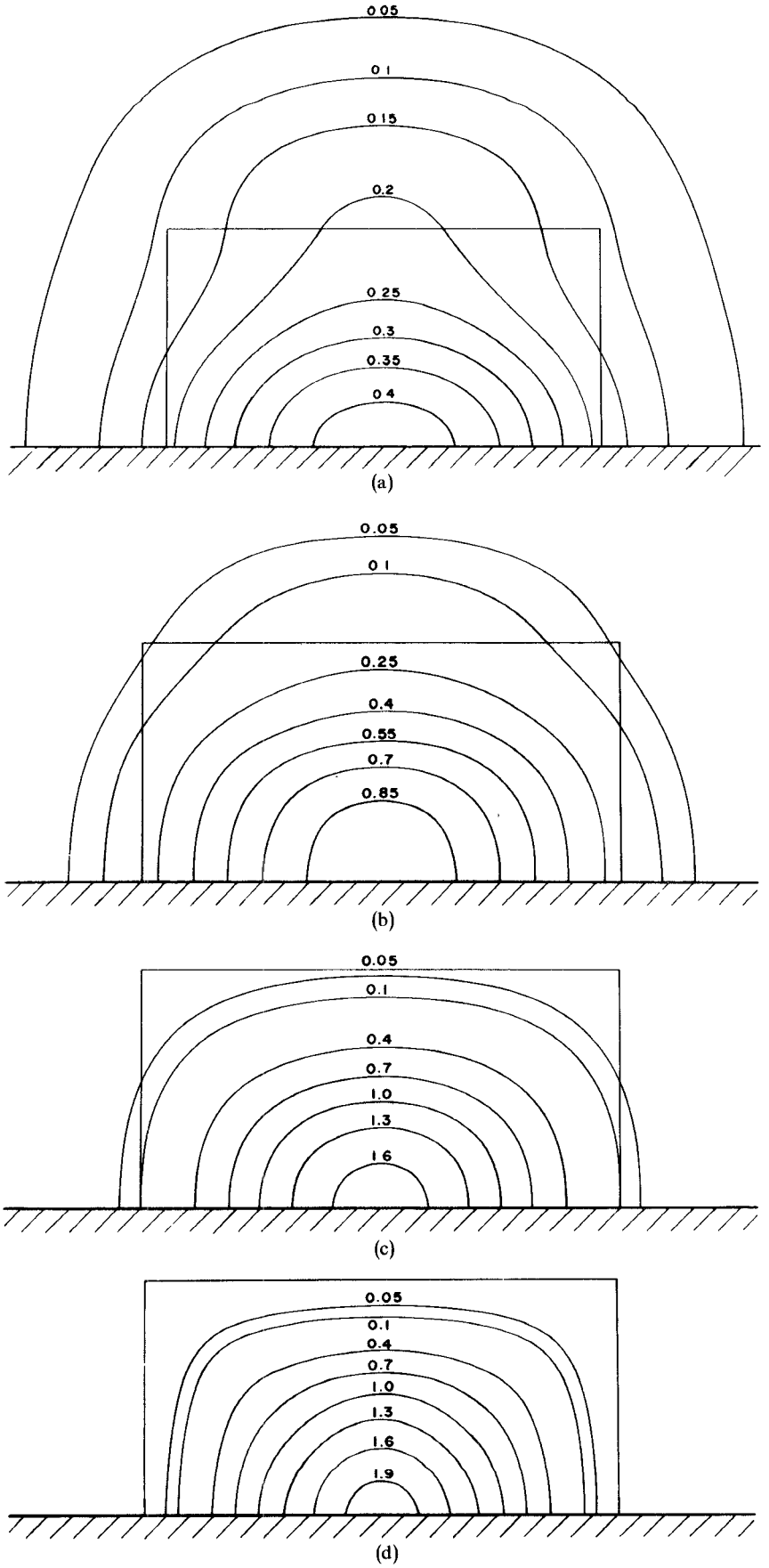

Fig. 4. Frequency dependence of the power distribution for the E_{11}^{y} mode in the rectangular dielectric image line with $d/c = 1.0$ and $\varepsilon_r = 2.5$ ($N_0 = 7$). (a) $k_0c = 1.5$. (b) $k_0c = 2.5$. (c) $k_0c = 5.0$. (d) $k_0c = 20.0$.

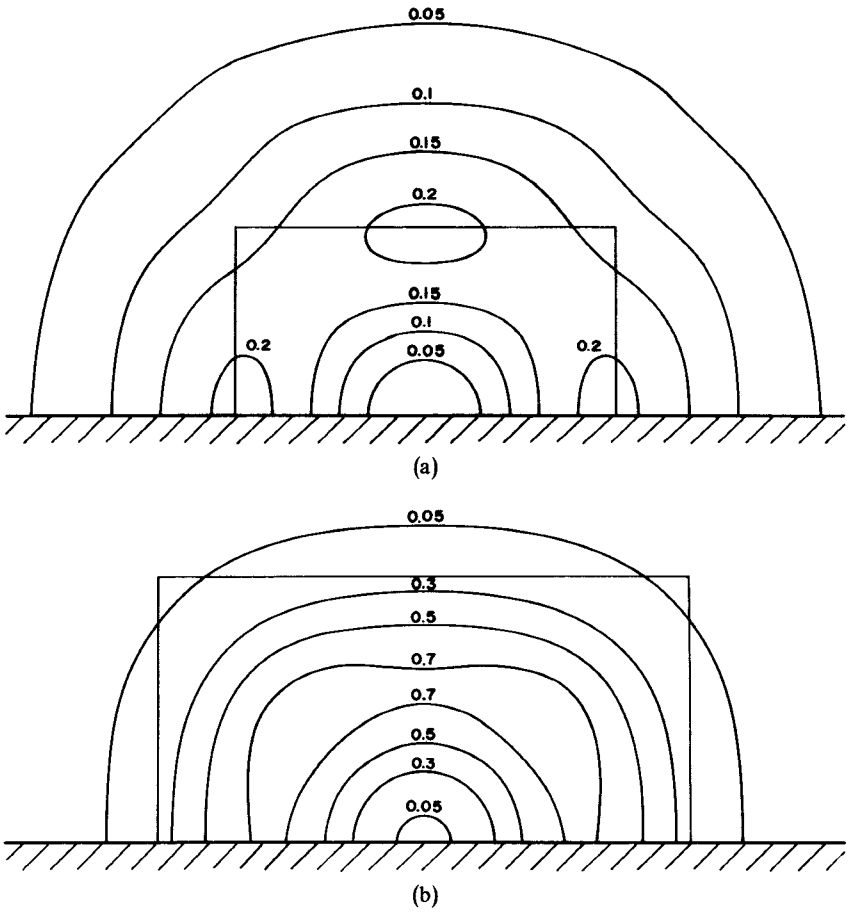

Fig. 5. Frequency dependence of the power distribution for the E_{21}^y mode in the rectangular dielectric image line with $d/c = 1.0$ and $\varepsilon_r = 2.5$ ($N_0 = 7$). (a) $k_0 c = 2.0$. (b) $k_0 c = 5.0$.

$k_z/k_0 = 1.0$, an increasingly large metallic wall is needed to maintain accuracy. In Fig. 3 results derived by other methods for the open image line are also presented. Since Marcatili's analysis [2] is based on an approximate mode matching method, the accuracy of his results for low frequencies near the transition region is questionable. On the other hand Pregla's analysis [4], which applies the variational method, is expected to give more accurate results than Marcatili's analysis. Agreement between our results and Pregla's are fairly good over a wide range of frequencies including the transition region. Fig. 4 shows the frequency dependence of the power distribution for the E_{11}^y mode. In this calculation $N_0 = 7$ was used. More terms are needed to compute field distributions than dispersion relations, because the latter is variational whereas the former is not. It is evident that the higher the frequency, the more the power is concentrated in the dielectric medium. Fig. 5 shows the frequency dependence of the power distribution for the E_{21}^y mode. The normalized frequency $k_0 c = 2.0$ in Fig. 5(a) is a little higher than the cutoff frequency $k_0 c = 1.83$. It is found that when the maximum of the power is located on the dielectric interface, the leakage of the power for the E_{21}^y mode occurs. On the other hand, the E_{11}^y mode seems to have no cutoff, because this mode is similar to the HE_{11}

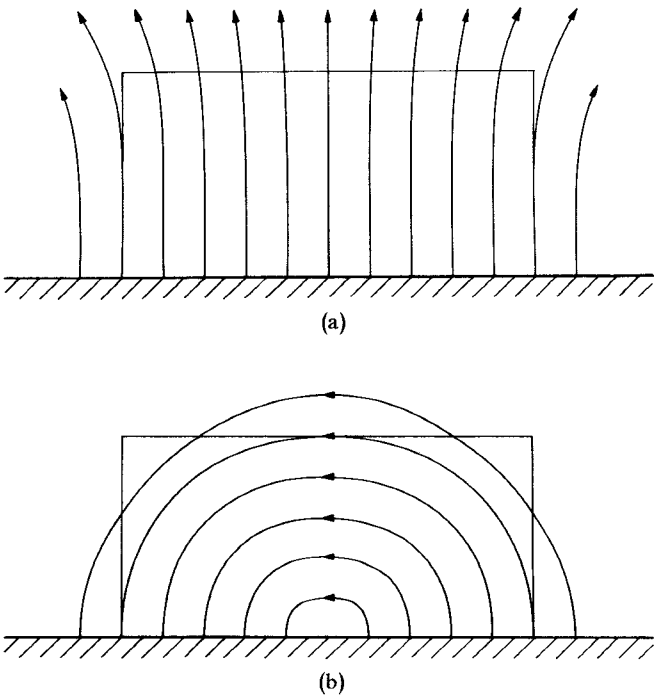

Fig. 6. Electric lines of force for the E_{11}^y and E_{21}^y modes corresponding to Fig. 4(c) and Fig. 5(b), respectively. (a) E_{11}^y mode. (b) E_{21}^y mode.

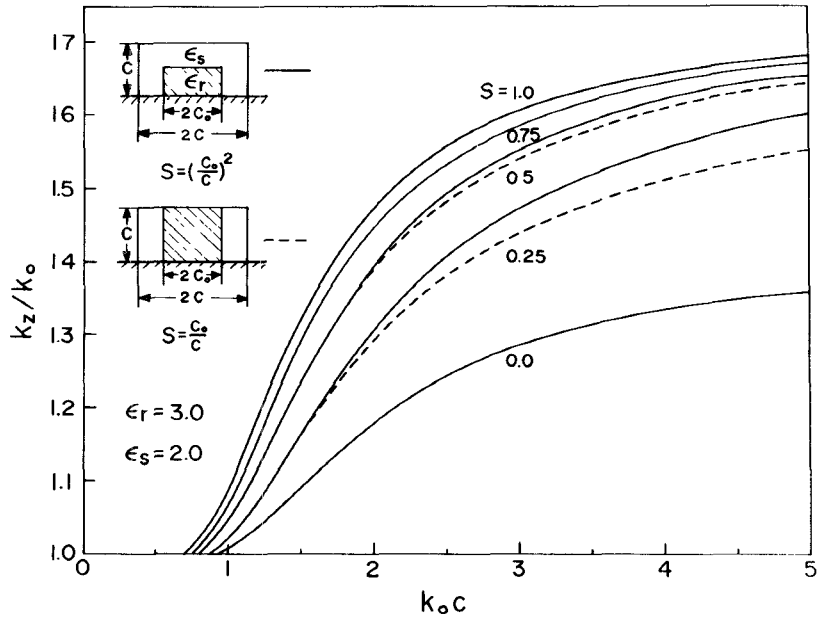

Fig. 7. Dispersion characteristics for the E_{11}^y mode in the cladded rectangular dielectric image line with $d/c = 1.0$, $\varepsilon_r = 3.0$, and $\varepsilon_s = 2.0$ ($N_0 = 5$).

mode in the circular dielectric waveguide. But, it is impossible to confirm this using our method because it is not an analytical exact solution. Fig. 6 shows electric lines of force for the E_{11}^y and E_{21}^y modes corresponding to Fig. 4(c) and Fig. 5(b). Although electric lines of force should refract at the dielectric–air interface, such phenomena do not appear in the computed results. This comes from expanding the field in the dielectric waveguides by continuous mode functions of the empty metallic waveguide. As pointed out by Goell [3], coupling between the E_{21}^y and E_{12}^y modes takes place in Fig. 5 with unit aspect ratio. It seems impossible to resolve this degeneracy using the present method.

Cladded Rectangular Dielectric Image Line

The cladded rectangular dielectric image line shown in Fig. 1(b) is a special case with $b_0 = 0$ in Fig. 2, and has a core of higher permittivity than the surrounding cladding. The transmission characteristics of this dielectric waveguide have not been studied extensively.

Fig. 7 shows the dispersion characteristics for the E_{11}^y mode in the cladded rectangular dielectric image line with $d/c = 1.0$, $\varepsilon_r = 3.0$, and $\varepsilon_s = 2.0$. As shown in Fig. 7, two cases of the structure are treated. The parameter S in Fig. 7 denotes the cross-sectional ratio of the core to the waveguide. When the normalized frequency is low, results for these two structures agree well. Fig. 8 shows the power distribution for the E_{11}^y mode at $k_0 c = 5.0$. In Fig. 8(a) and (c), the average relative permittivity in the cross section is 2.5, and the power is more concentrated in the core than Fig. 4(c). Since the field penetration in the air is less than the rectangular dielectric image line, this dielectric waveguide has the following advantages: a) the power carried may be isolated from the environment to some degree, b) bending losses may be more reduced than the rectangular dielectric image line.

Insulated Image Guide and Strip Dielectric Guide

The insulated image guide and the strip dielectric guide shown in Fig. 1(c) are special cases with $c_0 = 0$ and $d_0 = 0$ in Fig. 2, and the image line shown in Fig. 1(d) is a special case with $\varepsilon_r = \varepsilon_t$ in Fig. 1(c). The insulated image guide has a dielectric strip of higher permittivity than the substrate, while the strip dielectric guide has a dielectric strip of lower permittivity. Since most of the power is concentrated in the region of highest permittivity, these guides differ in the mechanism of propagation.

Fig. 9 shows dispersion characteristics for the E_{11}^y mode in these dielectric waveguides with $b_0/c = 1.0$ and $d/c = 1.0$. In Fig. 9 the results derived by McLevige *et al.* [14] for the insulated image guide are also presented. Their analysis is based on the method of an effective dielectric constant. Agreement between our results and theirs is good at high frequencies. Fig. 10 shows the frequency dependence of the power distribution for the E_{11}^y mode in the insulated image guide with $\varepsilon_r = 3.0$ and $\varepsilon_t = 2.0$. When the frequency is very high, the maximum power is located at the center of the dielectric strip and its field distribution is similar to that of the rectangular dielectric waveguide. The lower the frequency, the more the position of the maximum nears the ground plane. When the frequency is very low, its field distribution is quite different from the rectangular dielectric waveguide. Fig. 11 shows the frequency dependence of the power distribution for the E_{11}^y mode in the image line shown in Fig. 1(d). It is found that the field penetration in the air is very small, and the lower the frequency, the more the field penetrates into the substrate. Therefore, this dielectric waveguide has the advantage that the stringent requirements of size and edge smoothness of the dielectric strip are considerably relaxed. Fig. 12 shows the variation of the power distribution in these dielectric waveguides at $k_0 c = 5.0$ when the permitivities of the dielectric strip and

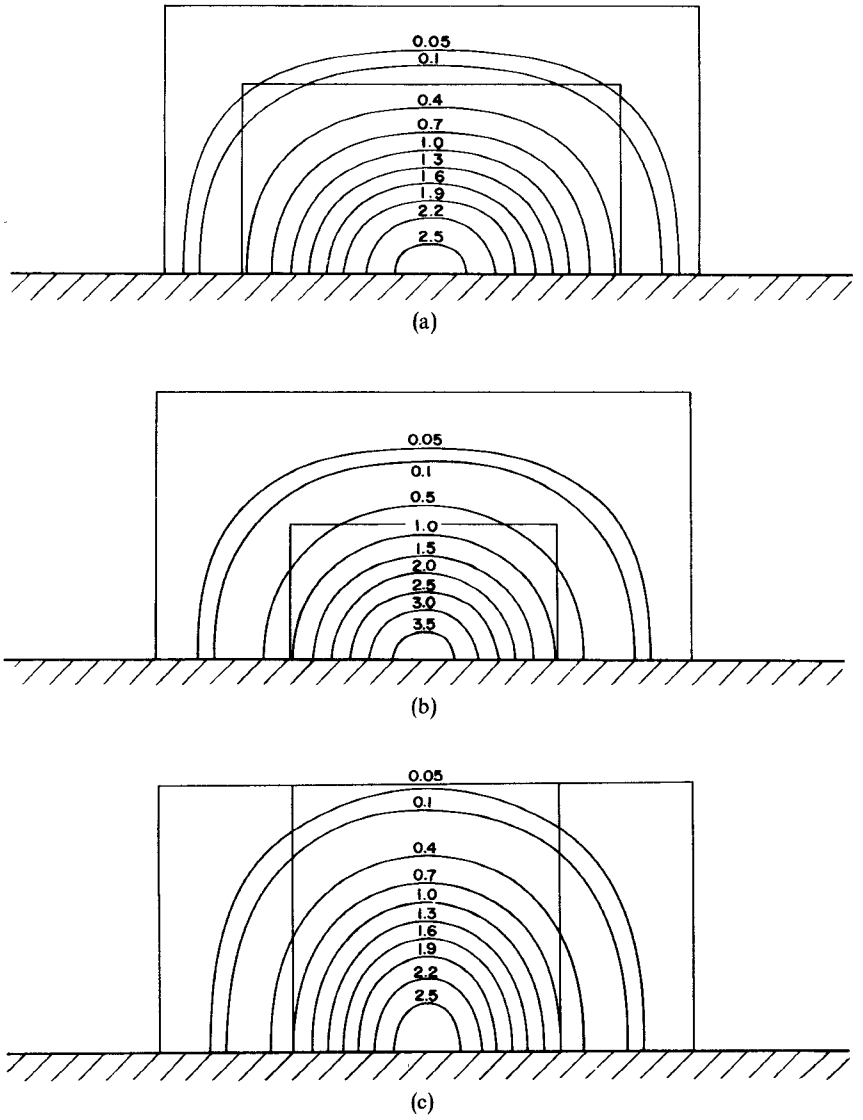

Fig. 8. Power distribution for the E_{11}^{y} mode in the cladded rectangular dielectric image lines with $d/c = 1.0$, $\varepsilon_r = 3.0$, and $\varepsilon_s = 2.0$ at $k_0 c = 5.0$ ($N_0 = 7$). (a) $c_0/c = d_0/d = 1/\sqrt{2}$. (b) $c_0/c = d_0/d = 1/2$. (c) $c_0/c = 1/2$, $d_0/d = 1$.

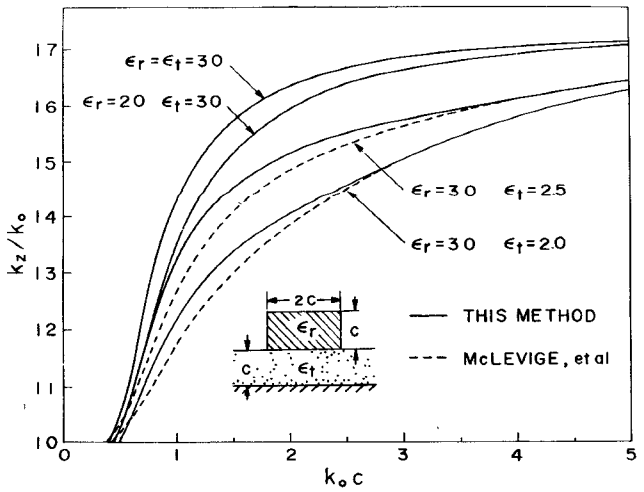

Fig. 9. Dispersion characteristics for the E_{11}^{y} mode in the insulated image guide and the strip dielectric guide with $b_0/c = 1.0$ and $d/c = 1.0$ ($N_0 = 6$).

the substrate are changed. We can well understand how the field penetrates into the substrate. It is found that the field distribution of the strip dielectric guide is similar to that of the image line shown in Fig. 1(d), and its field penetrates deeper into the substrate with increasing differences between the permitivities. From this fact, it is obvious that the dispersion characteristics of these two guides are quite similar as shown in Fig. 9. Results of these dielectric waveguides are useful in discussing the propagation characteristics in the slab coupled waveguide [11], including such special cases as the rib waveguide [9] and the strip loaded film waveguide [10], [12].

IV. Conclusion

Dielectric waveguides suitable for millimeter and submillimeter wave integrated circuits are analyzed by applying generalized telegraphist's equations. In this paper we treated the rectangular dielectric image line, the cladded rectangular

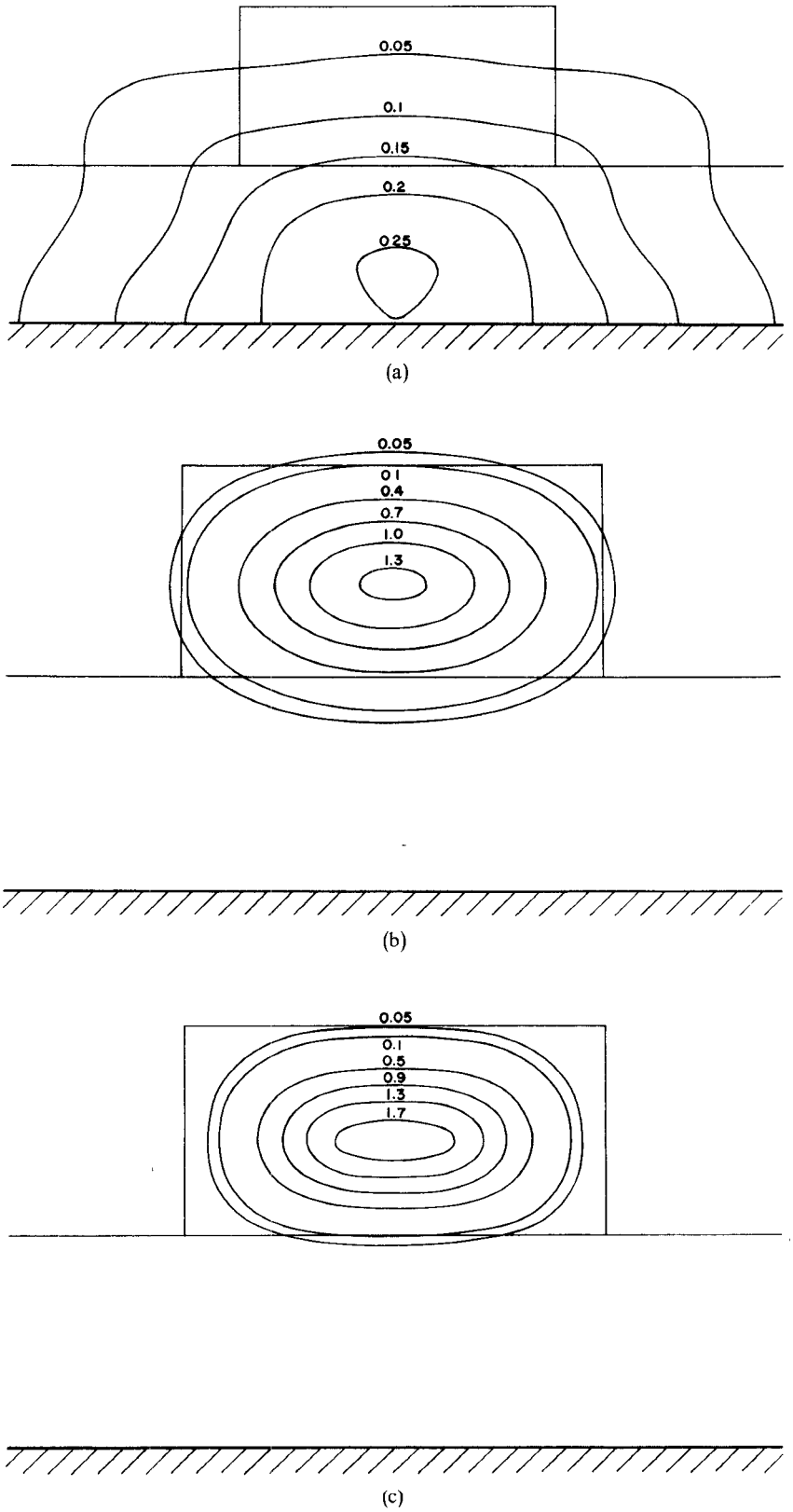

Fig. 10. Frequency dependence of the power distribution for the E_{11}^{y} mode in the insulated image guide with $b_0/c = 1.0$, $d/c = 1.0$, $\varepsilon_r = 3.0$, and $\varepsilon_t = 2.0$ ($N_0 = 7$). (a) $k_0c = 1.0$. (b) $k_0c = 5.0$. (c) $k_0c = 20.0$

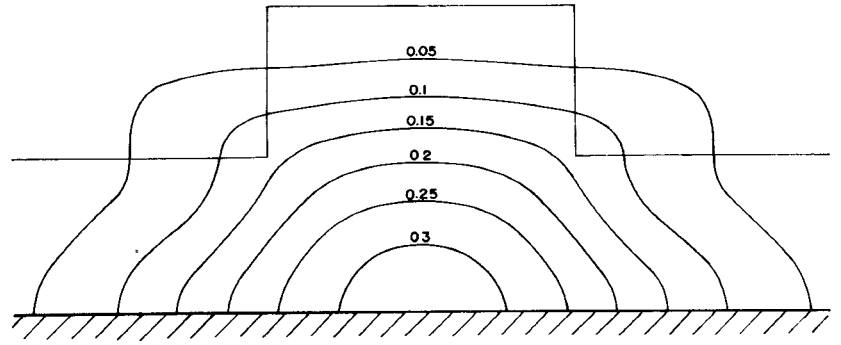

(a)

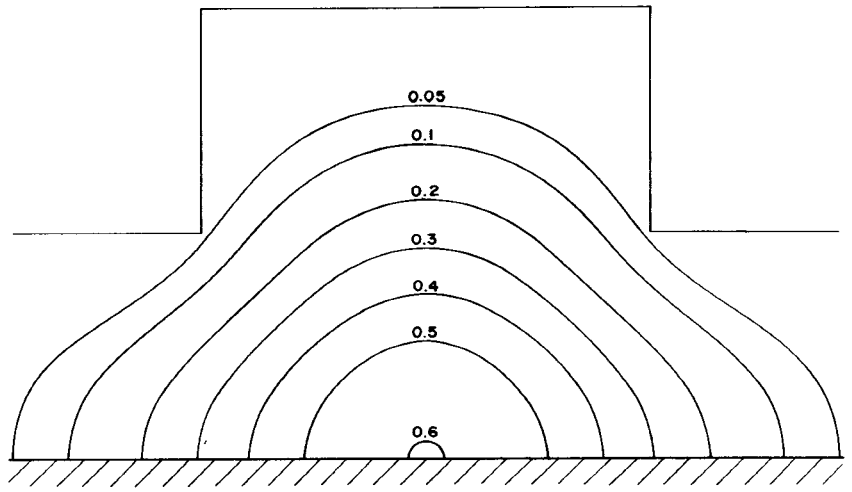

(b)

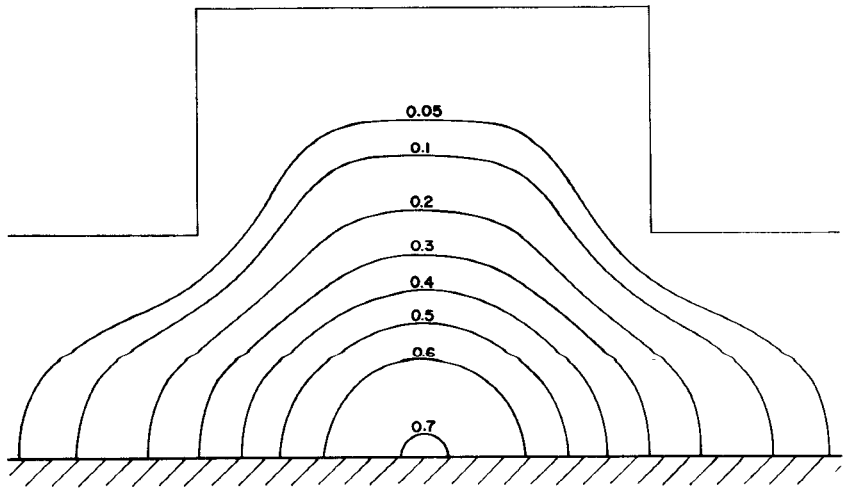

(c)

Fig. 11. Frequency dependence of the power distribution for the E_{11}^{y} mode in the image line shown in Fig. 1(d) with $b_0/c = 1.0$, $d/c = 1.0$, and $\varepsilon_t = 3.0$ ($N_0 = 7$). (a) $k_0c = 1.0$. (b) $k_0c = 5.0$. (c) $k_0c = 20.0$.

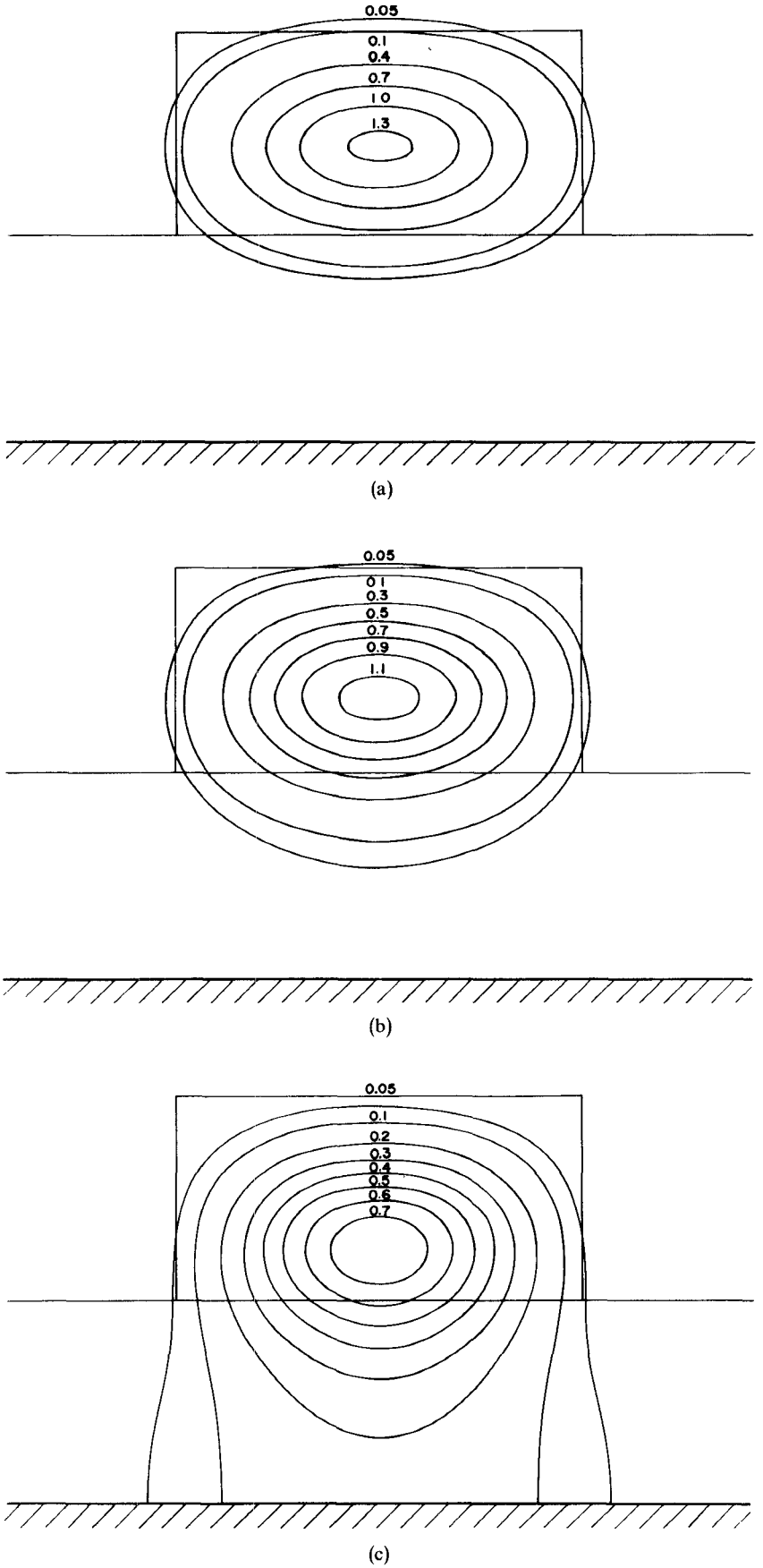

Fig. 12. Variation of the power distribution at $k_0c = 5.0$ when permittivities of the dielectric strip and the substrate are changed. The cross section is selected as $b_0/c = 1.0$ and $d/c = 1.0$ ($N_0 = 7$). (a) $\varepsilon_r = 3.0$, $\varepsilon_t = 2.0$. (b) $\varepsilon_r = 3.0$, $\varepsilon_t = 2.5$. (c) $\varepsilon_r = 3.0$, $\varepsilon_t = 2.75$.

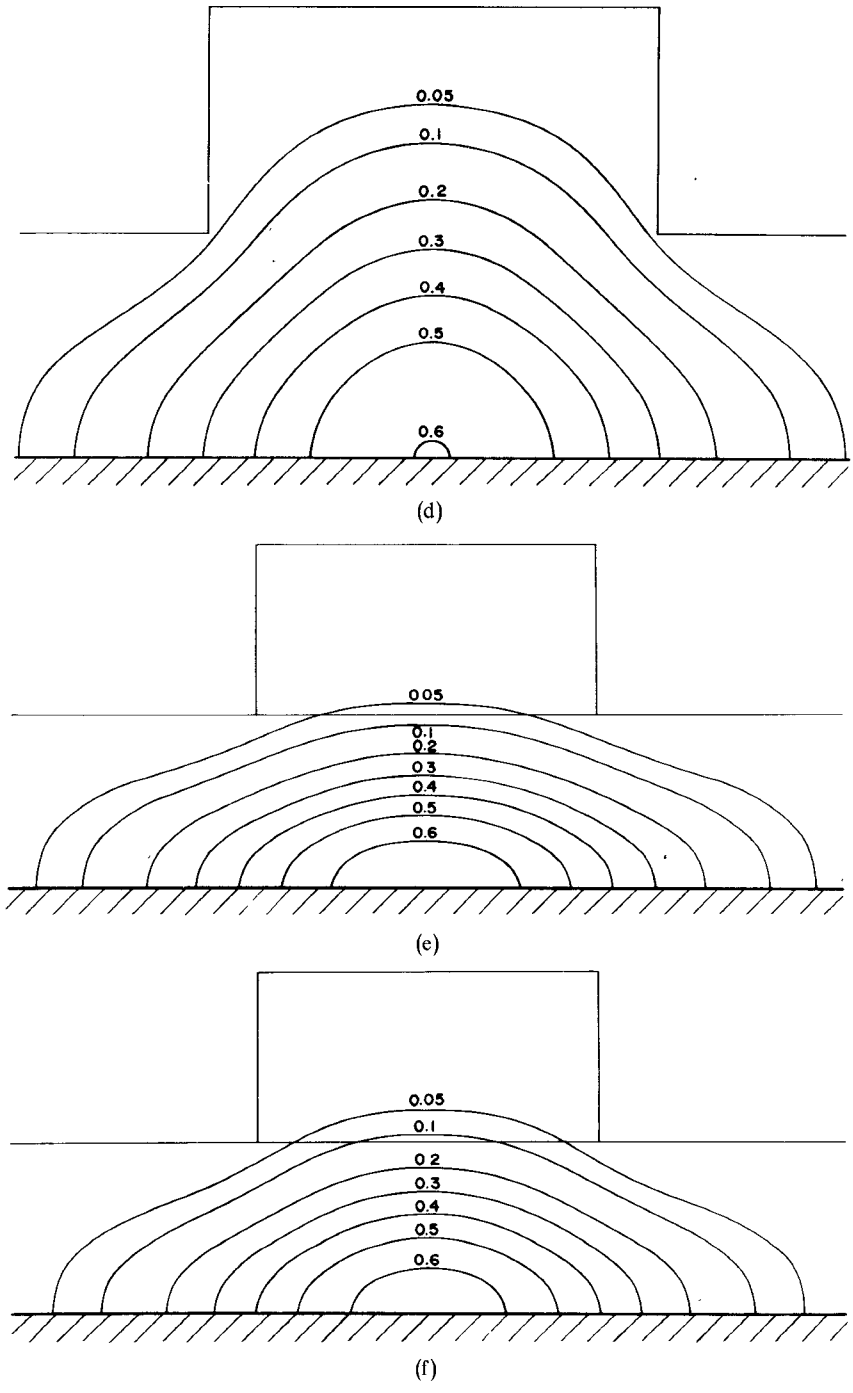

Fig. 12. (d) $\varepsilon_r = \varepsilon_t = 3.0$. (e) $\varepsilon_r = 2.75$, $\varepsilon_t = 3.0$. (f) $\varepsilon_r = 2.5$, $\varepsilon_t = 3.0$.

dielectric image line, the insulated image guide, and the strip dielectric guide shown in Fig. 1. The numerical results presented here include the dispersion characteristics, the lines of force, and the power distribution. Our dispersion characteristics are in good agreement with other theoretical results. It is shown that this analysis can give good results even for open dielectric waveguides with arbitrary dielectric profiles and cross sections even though the analysis is based on a closed waveguide model. Our results can be useful to understand the wave propagation in these dielectric waveguides, and may be applied to develop new waveguide systems.

Acknowledgment

The author wishes to thank Dr. K. Hongo for many helpful discussions. The numerical computations were carried out by FACOM 230-60 at Nagoya University.

References

[1] W. Schlosser and H. G. Unger, "Partially filled waveguides and surface waveguides of rectangular cross-section," in *Advances in Microwaves*. New York: Academic Press, 1966, pp. 319–387.
[2] E. A. J. Marcatili, "Dielectric rectangular waveguide and directional coupler for integrated optics," *Bell Syst. Tech. J.*, vol. 48, pp. 2079–2102, Sept. 1969.
[3] J. E. Goell, "A circular-harmonic computer analysis of rectangular

dielectric waveguides," *Bell Syst. Tech. J.*, vol. 48, pp. 2133–2160, Sept. 1969.
[4] R. Pregla, "A method for the analysis of coupled rectangular dielectric waveguides," *Arch. Elekt. Übertragung*, band 28, pp. 349–357, Sept. 1974.
[5] A. L. Cullen and O. Ozkan, "Coupled parallel rectangular dielectric waveguides," *Proc. Inst. Elec. Eng.*, vol. 122, pp. 593–599, June 1975.
[6] J. F. Heitmann, "Theory and fabrication of dielectric image lines and measurements in the frequency range from 26.5 to 40 GHz," *NTZ-Aufsätze*, vol. 28, pp. 279–284, Aug. 1975.
[7] K. Ogusu and K. Hongo, "Analysis of dielectric waveguides by generalized telegraphist's equations," *Trans. Inst. Electron. Commun. Eng. Jap.*, (Corresp.) vol. J60-B, pp. 358–359, May 1977
[8] ——, "Experimental investigation of dispersion characteristics in rectangular dielectric waveguides," *Trans. Inst. Electron. Commun. Eng. Jap.*, to be published.
[9] J. E. Goell, "Rib waveguide for integrated optical circuits," *Appl. Optics*, vol. 12, pp. 2797–2798, Dec. 1973.
[10] H. Furuta, H. Noda, and A. Ihaya, "Novel optical waveguide for integrated optics," *Appl. Optics*, vol. 13, pp. 322–326, Feb. 1974.
[11] E. A. J. Marcatili, "Slab-coupled waveguides," *Bell Syst. Tech. J.*, vol. 53, pp. 645–674, Apr. 1974.
[12] V. Ramaswamy, "Strip-loaded film waveguide," *Bell Syst. Tech. J.*, vol. 53, pp. 697–704, Apr. 1974.
[13] D. Marcuse, "Theory of the single-material fiber," *Bell Syst. Tech. J.*, vol. 53, pp. 1619–1641, Oct. 1974.
[14] W. V. McLevige, T. Itoh, and R. Mittra, "New waveguide structures for millimeter-wave and optical integrated circuits," *IEEE Trans. Microwave Theory Tech.*, vol. MTT-23, pp. 788–794, Oct. 1975.
[15] T. Itoh, "Inverted strip dielectric waveguide for millimeter-wave integrated circuits," *IEEE Trans. Microwave Theory Tech.*, vol. MTT-24, pp. 821–827, Nov. 1976.
[16] S. A. Schelkunoff, "Generalized telegraphist's equations for waveguides," *Bell Syst. Tech. J.*, vol. 31, pp. 784–801, July 1952.
[17] N. Marcuvitz, *Waveguide Handbook*. New York: McGraw-Hill, 1951, ch. 2.

Solutions of the Vector Wave Equation for Inhomogeneous Dielectric Cylinders—Scattering in Waveguide

GABRIELE CICCONI AND CARLO ROSATELLI

Abstract—**Some solutions of the vector wave equation for an inhomogeneous dielectric cylinder, suitable for numerical calculations of the scattered electromagnetic (EM) field in waveguide, are presented in cases where the cylinder axis is parallel, or perpendicular, to the incident electric field vector. The scattered field, given in terms of normal modes of the rectangular waveguide, permits easy determination of the transmission and reflection coefficients for the structure. The dielectric susceptibility may be considered as variable along the cylinder radius according to a parabolic function (Luneberg-type profile). Finally, numerical results of the scattered near field are presented for Teflon cylinders of different diameters, in the case of parallel polarization. They are compared with laboratory measurements in the microwave *X* band made as a reliability test of the computational program. The agreement between measured and computed values is satisfactory within a deviation of 10 percent in the whole frequency band.**

I. Introduction

SCATTERING and diffraction in free space by cylindrical objects of homogeneous and stratified dielectric, when the incident electromagnetic (EM) field is parallel or perpendicularly polarized, have been investigated by various authors [1]. The inhomogeneous case has also been treated for scattering by plasma columns [2].

The same problem in waveguide has been developed both for parallel incidence, by solving the wave vector equation in the case of inhomogeneous dielectric or plasma columns [3]–[5], and for perpendicular incidence, by using variational and Green's function techniques [6], [7].

In this paper, some exact solutions of the vector wave equation, in circular cylindrical coordinates and for homogeneous and radially inhomogeneous (Luneberg-type parabolic variable profile) complex permittivities, are presented in cases of parallel and perpendicular incidences of the EM field. These solutions have been expressed in a series of tabulated Bessel functions (homogeneous dielectric case) or in a series of confluent hypergeometric or Kummer's functions (inhomogeneous parabolic case). They have been found as suitable for developing numerical calculations of microwave scattering in waveguide.

Approximate values dependent on the truncation of the field series expansion may be estimated by the unitary condition of the scattering matrix.

The numerical results concerning the scattered near field

Manuscript received November 29, 1976; revised May 23, 1977.
The authors are with the Electrical Engineering Department, University of Genoa, Genoa, Italy.